New Developments for Improved Local Efficiency Parameter Imaging

Otwin Breitenstein
Max Planck Institute of Microstructure Physics, Hale, Germany

Abstract
This contribution reviews recent developments for imaging local efficiency-governing solar cell parameters, like the local series resistance, the local saturation current density, and the local short circuit current density. There are various definitions and measurement procedures for the local series resistance R_s, most of them relying on the simple model of independent diodes (one in each pixel), each of them being connected to the terminals by an independent series resistor. Each procedure and R_s definition correctly describes the local voltage drop for its particular measurement condition. However, until now there is no definition of a series resistance, which could describe the solar cell both in the dark and under illumination. Here, for the first time, such a definition is proposed, which divides the series resistance into a horizontal fraction, describing the distributed part of R_s including possible grid interruptions, and a vertical fraction basically describing the grid contact resistance. The second topic is the imaging of the local saturation current density J_{01}. This parameter can be mapped by dark lock-in thermography (DLIT) and photoluminescence (PL) imaging. However, the results of these two methods do not agree, local J_{01} maxima are imaged much stronger in DLIT than in PL evaluation. Here the reason of this discrepancy is resolved by performing 2-dimensional device simulations of a solar cell with well-defined J_{01} inhomogeneities. These simulations lead to simulated DLIT and PL images, which have been evaluated by generally accepted methods to retrieve the J_{01} distribution. It is found that only DLIT is able to image J_{01} correctly, apart from its inevitable thermal blurring effect, but PL systematically underestimates local J_{01} maxima. The reason is the too simple independent diode model, which underlies both methods but disturbs much more the PL than the DLIT evaluation. Finally two new LIT-based techniques for imaging the short circuit current density are introduced.

1. Introduction

No solar cell is really laterally homogeneous. Even in good monocrystalline silicon cells the effective series resistance is position-dependent, and at least in the edge region and below the grid contacts the local diode properties deviate from that in the free areas. In reality most solar cells show additional local inhomogeneities of the dark saturation current density of the first diode J_{01}, describing recombination in the bulk and at the surfaces, of that of the second diode J_{02} and its ideality factor n_2, describing recombination in the depletion region, and of the parallel resistance R_p, which has mostly local technological origins, see [1]. In particular multicrystalline (mc) silicon solar cells show strong inhomogeneities of J_{01} due to their inhomogeneously distributed crystal defects, leading to strongly inhomogeneous bulk lifetimes. Therefore, for understanding such inhomogeneous solar cells in detail and predicting the influence of certain defect regions on their efficiency, imaging methods for the basic solar cell parameters are necessary. The most successful methods until now are based on the evaluation of dark lock-in thermography (DLIT) images [2,3,4] and of photoluminescence (PL) images taken under various illumination and biasing conditions [5,6,7]. Both DLIT and PL evaluation until now rely on the independent diode model, hence it is assumed that each local diode (pixel) is connected to the terminals by its individual series resistor. In reality, however, most part of the series resistance of a solar cell is distributed. Both in the grid lines and in the emitter the current flows horizontally, and the corresponding resistances carry current contributions of many diodes. Another interesting technique is CELLO (solar CeLl, LOcal characterization (see e.g. [7,8]), which is a bias-, wavelength-, frequency-, and global illumination-dependent local modulated beam-induced current resp. voltage method and considers the distributed character of R_s. The local R_s concept of CELLO considers the local voltage as a linear response to the global external current; this was also applied to PL imaging [9].

Several attempts to apply these different imaging methods to one and the same cell have shown that the results agree with each other only qualitatively, but not quantitatively [10,11,12]. In this contribution the physical origins of these differences will be illuminated in detail and a possible way for a universal and comprehensive local characterization of solar cells will be sketched. First we will ask the question how a local series resistance is defined. Then the different previous concepts for describing the local series resistance R_s will be reviewed. It will turn out that none of these concepts is able to describe the local voltage drop both in the dark and under illumination correctly. Therefore here, for the first time, an alternative concept for describing the local R_s in solar cells will be introduced. Then the accuracy of DLIT- and PL-based J_{01} images is checked by evaluating simulated DLIT and PL images of a model cell having a well-defined distribution of J_{01}. It will be found that the previous PL-based evaluation systematically underestimates J_{01} in low lifetime regions, but DLIT images J_{01} correctly, apart from thermal blurring. Finally, some new methods for imaging the short circuit current density are introduced.

2. The local series resistance problem

2.1. Previous R_s concepts

All previous DLIT- and PL- (also electroluminescence, EL-) based solar cell analysis methods are based on the model of independent diodes. This model was first used to describe macroscopic regions of different lifetimes in the same solar cell [13], which indeed are electrically connected in parallel. Later on this concept was extended to each pixel of a solar cell and used to describe the local series resistance by Trupke et al. [14], and most other authors have adopted this concept. In this concept the

local series resistance $R_s(x,y)$ is defined as the local voltage drop $\Delta V(x,y)$ between the terminal voltage V and the local diode voltage $V_d(x,y)$, divided by the net local diode current density $J_d(x,y)$ (negative under illumination) flowing through the diode in position (x,y):

$$R_s(x,y) = \frac{V - V_d(x,y)}{J_d(x,y)} \quad (1)$$

Since $J_d(x,y)$ has the unit A/cm^2, this 'area-related' R_s has the unit Ωcm^2. The practical advantage of this concept is that this R_s does not depend on the area of the cells, hence it can be used directly in the 2-diode model formulated for current densities. For a homogeneous solar cell with area A, the series resistance in Ω can easily obtained from that in Ωcm^2 by dividing through the area A. For an inhomogeneous solar cell consisting from many elementary diodes (pixels) having different diode properties, this concept is equivalent to the 'independent diode' equivalent model of a solar cell shown in Fig. 1.

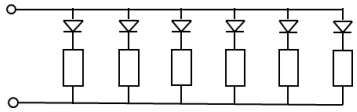

Fig. 1: Independent diode model of a solar cell

Hence, it is assumed here that an extended solar cell is a parallel connection of individual elementary diodes (pixels), each of them being connected to the terminals by its own series resistance. In reality, however, a solar cell has to be described by an at least 2-dimensional equivalent circuit like that in Fig. 2.

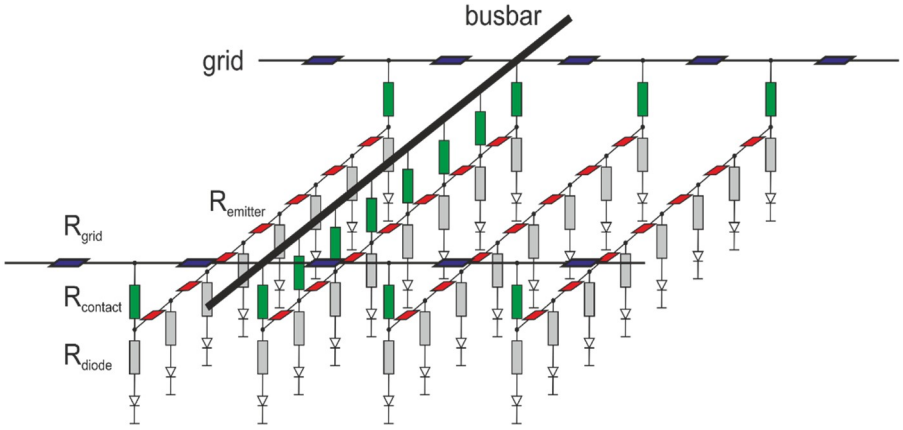

Fig. 2: More realistic equivalent circuit of a solar cell

Also this model is simplified. Here the busbar and the back contact are assumed not to contribute to the series resistance, and the lateral conduction in the bulk is neglected. For simplicity, here only the emitter resistors in current direction are drawn (from grid to grid), similar emitter resistors also exist perpendicular to these. The grid resistances R_{grid} and the emitter resistances $R_{emitter}$ carry horizontal currents. Hence, these are distributed resistances [15], for which the independent diode model certainly does not hold. Only the local diode resistors R_{diode} and the grid contact resistors $R_{contact}$ carry vertical currents through the diodes, hence they may be described as area-related resistances. Until now no results of imaging techniques have been fitted to an equivalent model like that in Fig. 2.

The most prominent example of an area-related resistance in the definition of (1) is the PL-based R_s [5,6,7,14]. The methods for calculating it, like all other PL and EL evaluation methods, are based on the general expression describing the local luminescence signal Φ in a position (x,y) of the cell showing a local diode voltage $V_d(x,y)$ [14,16]:

$$\phi(x,y) = C(x,y) exp \frac{V_d(x,y)}{V_T} + \phi_{PL,sc}(x,y) \quad (2)$$

Here $C(x,y)$ is the local luminescence calibration constant, V_T is the thermal voltage, and $\Phi_{PL,sc}(x,y)$ is the local PL signal under short circuit condition, which is due to the diffusion-limited carriers. For EL imaging this term is zero. Assuming the independent diode model, the basic evaluation formula is:

$$V_d(x,y) = V - \left(J_{01}(x,y) exp \frac{V_d(x,y)}{V_T} - J_p(x,y) \right) R_s(x,y) \quad (3)$$

Here $J_p(x,y)$ is the local photocurrent density, which is often assumed to be homogeneous and is zero for EL imaging. As a rule, the calibration constant $C(x,y)$ is measured from a low-intensity (usually 0.1 sun) PL image under open circuit (V_{oc}) condition. It is assumed that for this low intensity the horizontal balancing currents, which will be discussed below, are so low that in all positions $V_d(x,y) = V_{oc}$ can be assumed. If also the short circuit PL signal $\phi_{PL,sc}(x,y)$ at this intensity is measured, (2) may be resolved to $C(x,y)$. Then, at full illumination intensity, one or two other PL images under current load and the corresponding $\phi_{PL,sc}(x,y)$ image are measured. In the Trupke method [14] only one such image is necessary and a homogeneously assumed J_{01} is used, which may stem from V_{oc} or from dark I-V measurements. Then the result of the procedure is only $R_s(x,y)$. In the Glatthaar [5,6] and Shen methods [7] several (at least two) PL images under different current loads have to be measured, leading

to independent images of $R_s(x,y)$ and $J_{01}(x,y)$. Fig. 3 (a) shows a typical PL-R_s image of a multicrystalline solar cell. It shows the expected parabolic shape between the gridlines and the busbars, it nicely shows several cases of broken grid lines, and it is nearly not influenced by the well-known inhomogeneity of J_{01}, which is typical for mc-Si solar cells, see below. It will be discussed below that the reason for this independence is the fact that PL-R_s is measured under basically homogeneous current condition.

A second widely used R_s concept is so-called RESI-R_s (REcombination current and series reSIstance imaging [17]), which is the equivalent to PL-R_s for dark measurement conditions. Here the local diode voltage is measured by EL imaging and the local current density is measured by DLIT. This concept is often used in the DLIT-based local efficiency analysis by the "Local I-V" method [3]. Fig. 3 (b) shows the RESI-R_s image of the cell of Fig. 3 (a) in the same scaling range. We see basically the same details. However, we see some dark spots in the RESI-R_s image, which are not visible in PL-R_s, and around these spots RESI-R_s is somewhat higher than PL-R_s. As Fig. 3 (c) shows, these spots are in the positions of local maxima of the dark current density J, which may be called 'J_{01} shunts'. In the next Section it will be explained where these R_s minima come from.

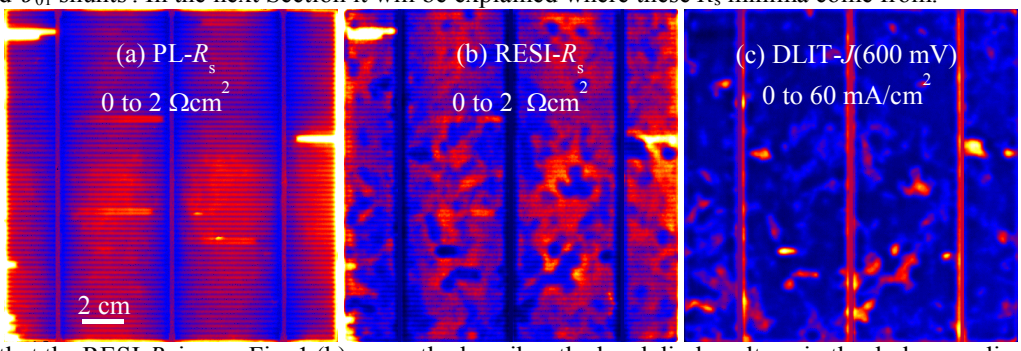

Fig. 3: (a) PL-R_s image of an industrial mc-Si solar cell, (b) RESI-R_s image of the same cell in the same scaling range, (c) dark current density image of this cell at 600 mV

The important fact here is that the RESI-R_s image Fig. 1 (b) correctly describes the local diode voltage in the dark according to eq. (1), as the PL-R_s image in (a) does it under illumination and current extraction. Since both images are different, there is obviously no R_s concept based on (1), which could describe the local voltage drop both in the dark and under illumination. The reason for this is the different current density distribution in both cases. In the dark this distribution is governed by the J_{01} distribution, which is very inhomogeneous in mc cells. Under illumination and current extraction (e.g. at the maximum power point mpp), this current density is dominated by the essentially homogeneous photocurrent (short circuit current) density and the dark current plays only a minor role. If the local R_s is based on the local current density, as in (1), hence if the independent diode model of Fig. 1 is applied, different R_s images must appear in the dark and under illumination and current extraction, and there is no possible R_s image describing both cases.

There are alternative R_s concepts, which do not rely on eq. (1) and may consider the distributed character of R_s. For example, the "linear response" model of Wagner et al. [9] considers the PL-measured local diode voltage under V_{oc} and under loaded condition, where the local diode voltages are here simply called V_d. The lateral balancing currents to be discussed below are assumed to flow under both conditions, only the additional local lateral voltage drop due to current extraction contributes to R_s. This concept indeed regards the distributed (horizontal) character of R_s. Here R_s is referred to the totally extracted current $I_{glob} < 0$, therefore this R_s has the unit of Ω:

$$R_s(x,y) = \frac{\{V_{oc}(x,y) - V_d(x,y)\} - \{V_{oc}(bb) - V_d(bb)\}}{I_{glob}} [\Omega] \qquad (4)$$

Here $V_{oc}(bb)$ and $V_d(bb)$ are the busbar voltages at V_{oc} and under current extraction, respectively. This term ensures that at the busbars $R_s = 0$ holds. As Fig. 4 (a) shows, also this series resistance is not disturbed by the local J_{01}. At present, this linear response concept is made explicit only for the evaluation of measurements under illumination. Nevertheless, the resulting R_s may also hold for the dark case.

Another R_s concept is the 'point-to-point' R_s concept, which also has been named 'geometrical Rs' [18], defined as the resistance between the busbars and a certain region in position (x,y) of the cell. This definition has to assume that all local diodes do not conduct, hence it holds exactly only under zero voltage condition. Also this R_s is defined in units of Ω, since this is a normal resistance between two points. However, because of the spreading resistance effect, in a 2-dimensional emitter this R_s is dependent on the size of the considered region in position (x,y). This does not hold for the 1-dimensional case, where this R_s is defined from a line to a line. Apart from mechanical probing methods, which hardly leads to an R_s image, this point-to-point R_s can be imaged e.g. by frequency-dependent CELLO Fast Fourier Transform (FFT) impedance analysis [8]. Here, at zero bias, with local laser excitation a pulsed photocurrent is injected at various frequencies. The local series resistance to the busbars, together with the local diode capacitance, yield an RC circuit acting as a low pass filter. Its corner frequency is a measure of the point-to-point R_s between position (x,y) and the busbars. Fig. 4 (b) shows a typical example of such an image of a mc solar cell. Also this image is not disturbed by J_{01}, since the local diodes are not conducting here. This R_s concept is

directly applicable neither to dark nor to illuminated conditions of a solar cell, since under both conditions the local diodes conduct. Their influence will be discussed in the following.

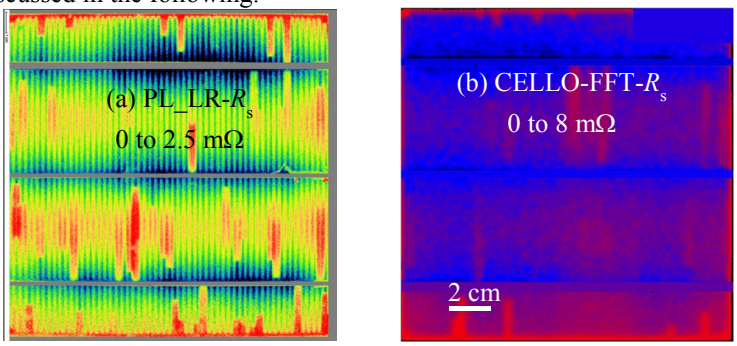

Fig. 4: (a) PL Linear Response (LR-) R_s image of an industrial mc solar cell [9], (b) CELLO-FFT-R_s image of another cell [12]

2.2. Basic properties of distributed series resistances

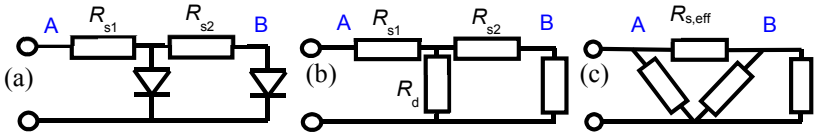

Fig. 5: (a) Chain of two resistance-coupled diodes to ground, (b) equivalent circuit of (a), (c) the same circuit after star-triangle transformation

For understanding the particular properties of distributed series resistances, the discussion of a linear chain of resistor-coupled diodes to ground is useful. In Fig. 5 (a) the chain consists of only two diodes and two series resistors R_{s1} and R_{s2}. Let us ask for the effective resistance between positions A and B. Under a certain forward biasing condition the two diodes may be described as equivalent diode resistances R_d, see Fig. 5 (b). These resistances, which may be defined as d.c. or as a.c. resistances, yield a star between positions A and B. This star may be converted into a triangle by the well-known star-triangle transformation, see Fig. 5 (c). Then the 'real' effective coupling resistance $R_{s,eff}$ between A and B is:

$$R_{s,eff} = \frac{R_{s1}R_{s2}+R_{s2}R_d+R_dR_{s1}}{R_d} \qquad (5)$$

Hence, only for infinitely large R_d, which corresponds to the point-to-point measurement condition at 0 V bias, $R_{s,eff} = R_{s1} + R_{s2}$ holds, as it could be expected. Under forward bias $R_{s,eff}$ becomes larger than this value, hence the coupling between points A and B becomes weaker. In the limit of $R_d \Rightarrow 0$, which corresponds to high injection condition, $R_{s,eff}$ tends to become infinite, hence then the two positions A and B are effectively decoupled from each other. This means that, in a circuit containing distributed series resistances and diodes to ground, the effective series resistance increases as the diode resistance R_d decreases.

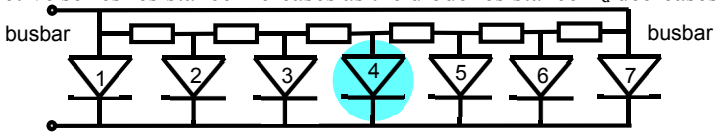

Fig. 6: Chain of 7 resistance-coupled diodes to ground. Diode No. 4 may or may not show an enhanced I_{01} (inhomogeneous resp. homogeneous case)

In Fig. 6 another resistance-coupled diode chain is shown, which consists of 7 diodes to ground coupled by series resistances, which are here all assumed to be the same. Also the saturation currents I_{01} of all diodes are assumed to be the same except that of diode #4. Two cases are considered here, namely the 'homogeneous' case, where also diode #4 has the same I_{01} as the other diodes, and the 'inhomogeneous' case, where diode #4 has the 3-fold I_{01} as the other diodes, thus yielding a 'I_{01} shunt'. The left and the right edge of the diode chain are connected to the applied bias V, which is her $V = 0.6$ V, just as in the case of a gridline between two busbars. Fig. 7 shows the simulation results for this circuit in full lines for the homogeneous case and dashed lines for the inhomogeneous one. In (b) it is visible that, in the inhomogeneous case, the current of diode 4 more than doubles compared to the neighboring diodes. This current would indeed be measured by DLIT, which calculates the current as the dissipated power (density) divided by the local diode voltage. However, in (a) we see that the voltage drop between the busbars (diodes 1 and 7) and this diode #4 increases only by 40 % in the inhomogeneous case. This is due to the resistive interconnection between all diodes, which distributes the voltage drop of the additional current of diode #4 also over the neighboring diodes, as can be seen in (a). With other words: In the inhomogeneous case additional lateral balancing currents exist in the emitter due to the local voltage differences, which are not regarded in the independent diode model. Under open circuit condition only these lateral balancing currents flow, which are responsible for the difference between the local diode voltages under this condition and their individual (isolated) V_{oc}. If R_s is measured after (1) by this voltage drop divided by the local current (density), the RESI-R_s curves in (d) appear. In the homogeneous case this RESI-R_s shows a nice parable, as expected, but in the inhomogeneous case R_s oscillates. In shunt position R_s is decreased and left and right of it it is even increased. The decrease in shunt position is due to the fact that the voltage drop in shunt position does not increase proportional to the local current density. The increase left and right of the shunt is due to the current reduction there (see b), in spite of the higher voltage drop in these positions (see a). These properties will be confirmed in our 2D simulations in Section 3. This

shows that the oscillation of RESI-R_s around a local shunt may be taken as an artifact coming from the inappropriate definition of R_s after (1). If the local diode current is calculated for PL-R_s, if measured at sufficiently low voltage (dark current is negligible), in the same definition the "PL-R_s, low voltage" curve in (f) appears, both for the homogeneous and inhomogeneous case. This curve exactly matches the RESI-R_s curve for the homogeneous case. Hence, in the homogeneous case, PL-R_s and RESI-R_s are equivalent, but not in the inhomogeneous case. In (f) also the geometrical R_s is displayed, which also yields a parable, independent on the diode properties. The absolute values are lying below that of PL-R_s, since in the latter case current contributions of several diodes are flowing across the resistors, see [18]. Also EL can be evaluated to yield a local R_s after (1), assuming the validity of the Fuyuki approximation [19], leading to the curves in (e). Again, in the homogeneous case the result is the same as for PL-R_s, but here the inhomogeneous case differs only slightly from the homogeneous one. The local currents according to this EL evaluation are shown in (c). These currents deviate significantly from the real diode currents in (b). The same would hold if the dark current is measured under illumination by PL after [5,6,7]. This means that luminescence techniques, if their evaluation is based on the independent diode model, systematically underestimate local dark current maxima in solar cells. The reason is the too simple circuit model applied in these evaluations, which does not properly take into account the influence of additional horizontal balancing currents, as they inevitably appear in inhomogeneous solar cells. Only for homogeneous solar cells PL-R_s appears correct, but then it is not interesting at all.

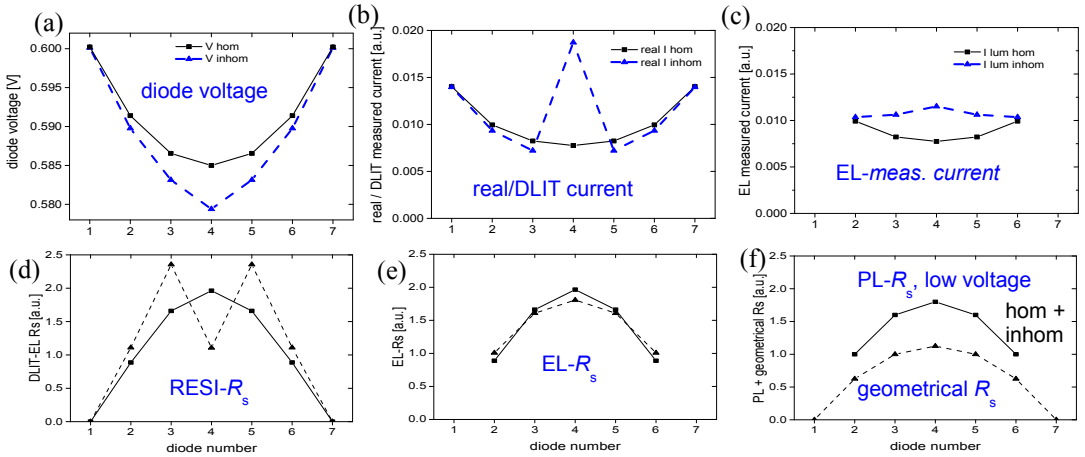

Fig. 7: Simulation results of the circuit of Fig. 6, see text. Full lines: homogeneous case, dashed lines: inhomogeneous case (diode #4 shows 3 times higher I_{01})

2.3. An alternative R_s concept

Equivalent model circuits like that in Fig. 2, which contain separate resistances for horizontal and vertical current transport, are often used for 2-dimensional finite element solar cell simulations if the local diode parameters are known, see e.g. [16,20]. We also have used a similar model circuit for simulating DLIT, PL, and EL images as shown in Section 3 of this contribution. However, according to the knowledge of the author, nobody ever has tried to fit experimental LIT- or luminescence-based images to the parameters of such a model. We have started to do this, based on one EL-based local diode voltage image $V_d(x,y)$ and one DLIT-based local current density image $J(x,y)$, both measured at the same applied bias of, in this case, 600 mV. Of course, these two independent data sets do not allow us to fit all resistances and diode parameters of the circuit. Therefore some additional simplifications have to be made. Here we assume that the vertical diode resistances R_{diode} and the emitter resistances $R_{emitter}$ in Fig. 2 are distributed homogeneous. Moreover we use the single diode model with an ideality factor of 1, hence we describe the local diodes only by their J_{01}. Finally, we assume that also the grid resistances are essentially homogeneous, except in some positions of grid interruption, see below. Hence, our free local parameters are the local J_{01} and the contact resistances $R_{contact}$. From an evaluation of the latter image we obtain information on the homogeneous value of R_{grid}, and we clearly see the positions of interrupted gridlines, see below. At the end we will have the local R_{grid} image and the local $R_{contact}$ image, which separately describe the voltage drops due to horizontally and vertically flowing currents.

The local values of J_{01} appear directly from the local diode voltages and the local current densities:

$$J_{01}(x,y) = J(x,y) exp \frac{-V_d(x,y)}{v_T} \quad (6)$$

Details of the procedure for fitting $R_{contact}$ will be presented in a separate publication. The principle is that we sum up the DLIT-measured vertical diode currents on their way in lines in the emitter to the grid lines, leading to the horizontal emitter current density between the gridlines. Then we sum up the local currents from these lines in the grid lines to the corresponding busbars, leading to the local horizontal grid currents. For calculating these grid currents, not only the local diode currents contribute, but also the net current flowing in the emitter perpendicular to the grid lines, if neighboring grid lines are at different potentials. Hence, here really the 2-dimensionally distributed series resistance in the cell is regarded. Then, assumed that we know $R_{emitter}$ and R_{grid} (the latter at the beginning is also assumed to be homogeneous), we may calculate the local V_{grid} and $V_{emitter}$. From the difference between $V_{emitter}$ and V_{diode}, with a certain assumed R_{diode}, we may calculate $R_{contact}$. As will be explained below, this

image is used to estimate the homogeneous value of R_{grid}, and the grid interruptions visible in this image are used to manually correct R_{grid} in these positions.

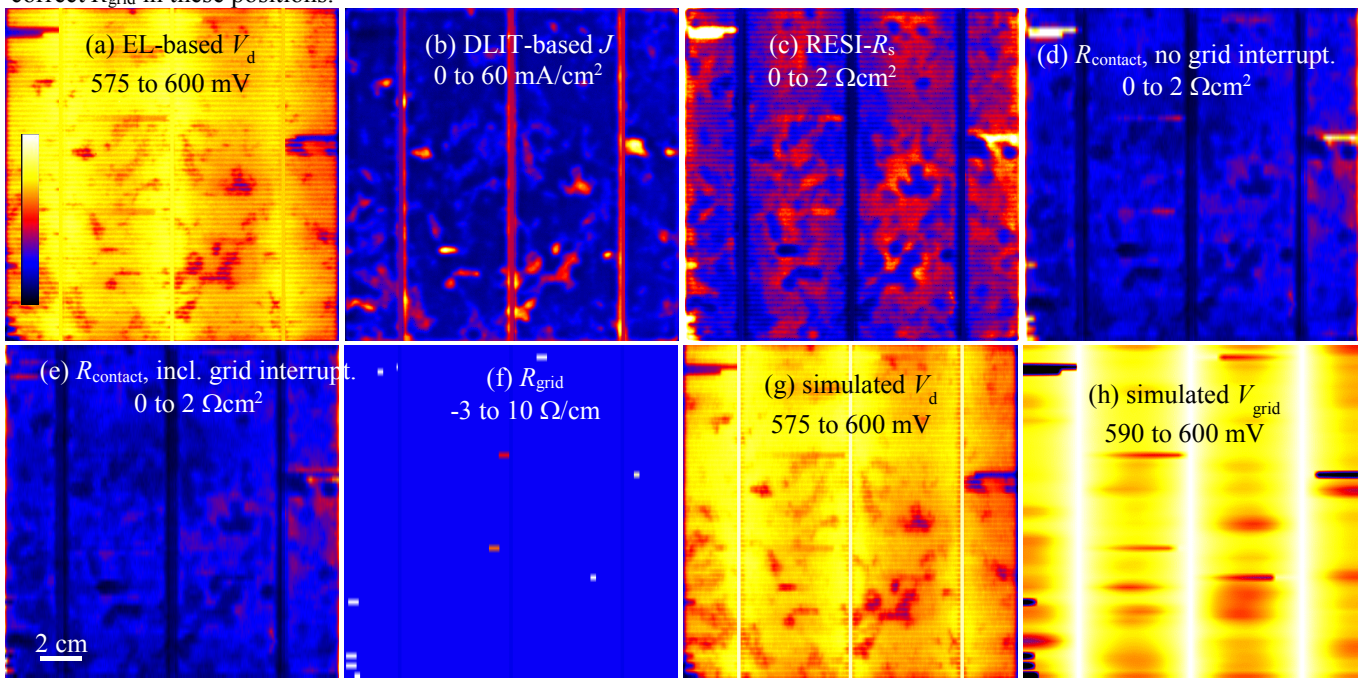

Fig. 8: (a) Local diode voltage image, obtained from EL at 600 mV, (b) local current density image, obtained from DLIT at 600 mV, (c) RESI-R_s image obtained from (a) and (b), (d) image of R_{cont} assuming no grid interruptions, (e) image of R_{cont} including grid interruptions, (f) image of R_{grid}, including the interruptions, (g) image of the local diode voltage simulated including grid interruptions, (h) simulated local grid voltage including grid interruptions

In Fig. 8 the two input images $V_d(x,y)$ (a, from EL) and $J(x,y)$ (b, from DLIT), both taken at 600 mV and 25 °C, together with some evaluation and fitting results are shown for the same cell as used for Fig. 3. Fig. 8 (c) shows the RESI-R_s image, which was already shown in Fig. 3, together with the current density image. The RESI-R_s image contains the influences of the broken gridlines (bright horizontal stripes, the influence of the grid resistance (a general parabolic profile between the busbars, with minima at the busbars), and possible real inhomogeneities of the grid contact resistance. In addition we see in the RESI-R_s image local minima (dark spots) in the positions of J_{01} shunts, which appear bright in the current density image (b). It was explained above in the discussion of Fig. 7 where these dark spots come from. Fig. 8 (d) shows the $R_{contact}$ image under the assumption of a homogeneous R_{grid}. As expected, $R_{contact}$ is lower than RESI-R_s since it does not contain the grid resistances anymore. This image is first used to optimize the (still homogeneous) value of R_{grid}, until (in homogeneous cell regions) a possible general parabolic profile of $R_{contact}$ between two busbars disappears. If R_{grid} is chosen too low, we see a positive parabolic profile between two busbars, and if it is chosen too high a negative one. Then the bright horizontal stripes in the $R_{contact}$ image are used to identify broken gridlines. In the suspect positions R_{grid} is manually increased until the bright stripes disappear. Fig. 8 (e) shows the $R_{contact}$ image after this procedure, and (f) shows the resulting R_{grid} image. We see that in the different positions different values of the remaining R_{grid} have to be assumed until $R_{contact}$ becomes homogeneous in the corresponding positions. Fig. 8 (g) shows the local diode voltage image simulated by applying the local J_{01}, $R_{contact}$, and R_{grid} data into the circuit model of Fig. 2. We see a very good correspondence to the input image of Fig. 8 (a).

Here, for the first time, DLIT and EL images are fit to a physically more meaningful solar cell equivalent circuit model. The influences of the grid resistance, grid interruptions, and real inhomogeneities of $R_{contact}$ can be separated now from each other. The method is not yet perfect at the moment. For example we still see local minima of $R_{contact}$ in the positions of local current maxima, and the resulting $R_{emitter}$ is still lower than expected. However, these minima are already weaker than in the RESI-R_s image, and we hope to get rid of them and obtain a more realistic $R_{emitter}$ by introducing further improvements of the method. It is hoped and will be checked soon how correct this model describes also the illuminated case.

3. The J_{01} problem

The definition of the local J_{01} is out of question, this is really a scalar area-related parameter, where the influences of all pixels add up across the cell surface. The only open point is here that the results of J_{01} imaging performed by DLIT and PL imaging disagree. This is demonstrated in Fig. 9 showing two of such J_{01} images of the cell also used for Figs. 3 and 8 in the same scaling range in (a) and (b). We have extensively investigated the origin of this discrepancy by 2-dimensional cell

simulations in [21] and have presented a proposal to solve the problem for PL in [22]. Here only our procedure is described and the most important results are presented.

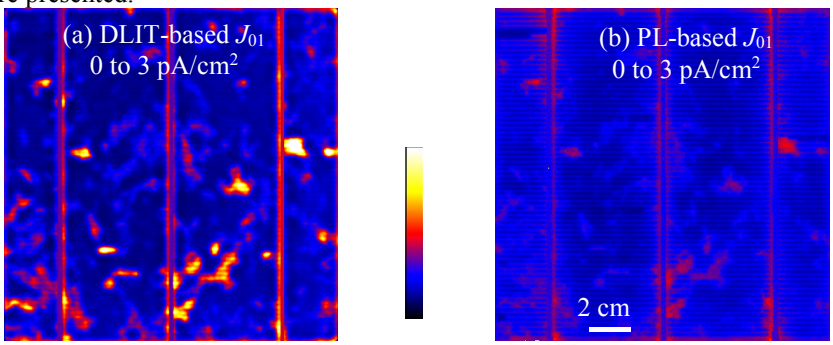

Fig. 9: (a) DLIT-J_{01} image of an industrial solar cell, (b) conventional PL-J_{01} image of this cell

We have performed 2-dimensional finite element device simulations on a model solar cell containing well-defined inhomogeneities of J_{01}. The cell was a 52x2.6 mm^2 sized symmetry element of a conventional 3-busbar cell, which is the area between two busbars left and right and two gridlines at the top and at the bottom. The grid is a square array with a pixel size of 130 µm. The used equivalent circuit is similar to that in Fig. 2, but somewhat more elaborate. For example, here we explicitly regarded the back contact resistance and horizontal current flow in the base in both directions, we also consider resistances parallel to the gridlines in the emitter, and we also consider a photo current. The latter is deliberately assumed to be homogeneous, because we want to study only the influence of an inhomogeneous J_{01} here. We have tried to select the circuit elements as realistically as possible for an industrial solar cell. In most of the area J_{01} was assumed to be homogeneously 1 pA/cm^2. Only in three regions, two close to the busbars and one in the middle of the model cell, J_{01} was assumed to be 3 pA/cm^2, thus yielding J_{01} shunts in these positions. This cell was simulated by a software based on Ngspice [23,16]. First we have simulated DLIT and PL images of this cell belonging to various biasing and illumination conditions. Then these realistically simulated images were evaluated according to well-accepted methods, which are 'Local I-V' for DLIT evaluation [3] and C-DCR for PL evaluation [5], leading to retrieved J_{01} distributions and also to RESI- and PL-R_s images.

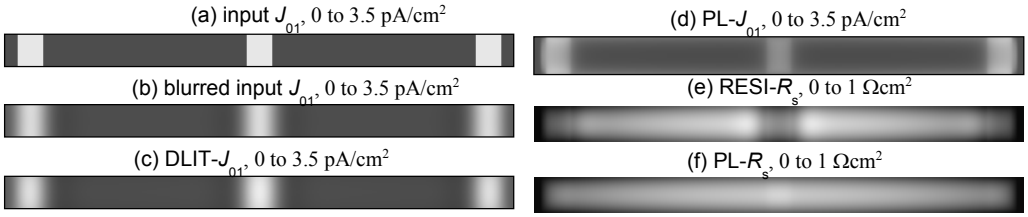

Fig. 10: (a) input J_{01} image of a model cell, (b) blurred input J_{01} image, (c) retrieved DLIT-J_{01}, (d) PL-J_{01}, (e) RESI-R_s, (f) PL-R_s images of this cell

The most important results of these simulations are collected in Fig. 10. Fig. 10 (a) shows the assumed input distribution of J_{01} in this cell. In (b) this input J_{01} distribution is shown blurred, using the same blurring point spread function as for simulating the DLIT images. Fig. 10 (c) and (d) show the DLIT- and PL-based retrieved J_{01} images. We see that, of course, the DLIT-based image (c) is blurred, but it nicely corresponds quantitatively to the blurred input J_{01} image in (b). In the PL-based J_{01} image (d), however, the J_{01} shunts appear clearly too weak. While the homogeneous value of J_{01} of 1 pA/cm^2 is imaged correctly by PL, the maximum of J_{01} in the middle of the cell is only 1.8 pA/cm^2 instead of the expected 3 pA/cm^2. Hence, the increase of J_{01} in shunt position is measured by PL as only by 80 % instead of the expected 200 %. This exactly corresponds to the simulation of the 1-dimensional diode chain in Fig. 7 and to the experimental results in Fig. 9. Fig. 10 (e) and (f) show the RESI-R_s and the PL-R_s images obtained from these simulation. Again, in correspondence to the results in Figs. 3 and 7, the RESI-R_s image (e) shows local minima in J_{01} shunt positions and maxima besides, whereas the PL-R_s image (f) is nearly not disturbed by the inhomogeneity of J_{01}. The result of these simulations is that, in accordance with the qualitative results obtained on a linear diode chain in Fig. 7, the evaluation of PL images of inhomogeneous solar cells by methods relying on the model of isolated diodes leads to wrong results of J_{01}. Local maxima of J_{01} are systematically underestimated in these PL evaluations. The reason for this has been explained in the discussion of Fig. 7. The isolated diode model assumes that, for a given value of R_s, the local current density is proportional to the local voltage drop. In a device with a horizontally distributed series resistance, however, in regions of locally increased current, this voltage drop is considerably smaller than expected in this simple model due to the resistive interconnection of neighboring diodes, leading to inevitable horizontal balancing currents. The DLIT evaluation also relies of the independent diode model, but here the local current densities are measured much more directly by the dissipated power density. Therefore this evaluation leads to realistic local J_{01} data, apart from the inevitable thermal blurring effect.

The linear response PL evaluation method of Wagner et al. [9] does not deliver any information to a local J_{01} but only to R_s. However, there are two other alternative methods for evaluating PL images, which are the differential luminescence imaging technique of Rau et al. [24] and the Laplacian-based PL evaluation method proposed by Glatthaar et al. [6]. The Rau method

relies on the evaluation of a differential PL image (the PL difference between two nearby lying voltages) and the net PL image (PL image minus J_{sc}-PL image) at this voltage and is based on the extended reciprocity theorem of Wong and Green [25]. It was hoped that this kind of evaluation could overcome the limitations of the isolated diode model. The Laplacian method of Glatthaar is based on the fact that, for a given emitter sheet resistivity, the second derivative of the local emitter voltage in horizontal current direction (which in two dimensions is the Laplacian operator) is proportional to the local diode current density. We have simulated also these two methods on our model solar cell with the results shown in [22]. The result was that the differential PL imaging technique of Rau et al. also does not lead to correct images of J_{01} if it is distributed inhomogeneously. However, the Laplacian method indeed has the potential to image J_{01} correctly. Nevertheless, when we applied this method on a real solar cell, again the local J_{01} maxima appeared too weak. This had been observed already by Glatthaat et al. [6]. We believe that this effect is caused by some optical blurring (cross-talk between neighboring pixels) occurring in the detector of the Si-based camera used for PL and EL imaging, see Walther et al. [26]. We hope that, by considering this effect, we may improve the accuracy of Laplacian-based PL evaluation, as well of the alternative R_s evaluation described in Sect. 2.3.

4. LIT-based J_{sc} imaging

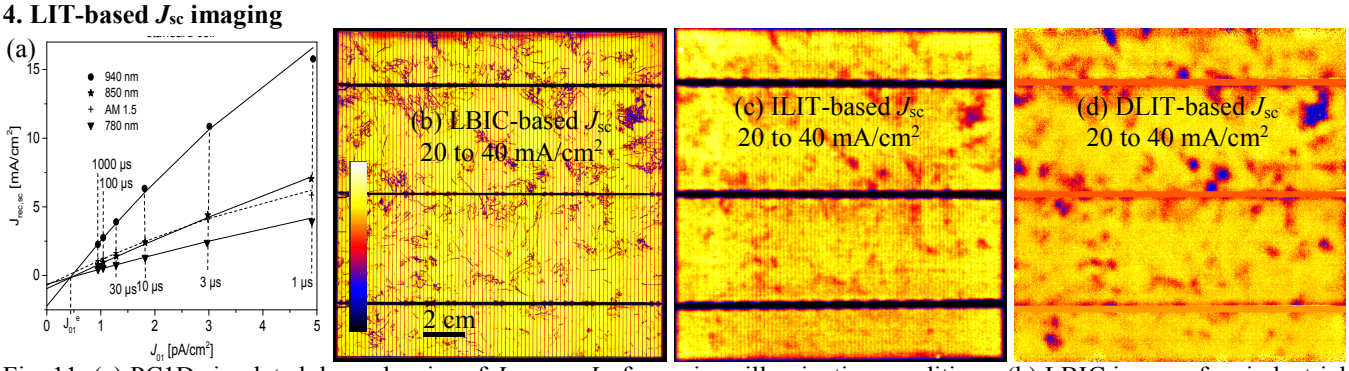

Fig. 11: (a) PC1D simulated dependencies of $J_{rec,sc}$ on J_{01} for various illumination conditions, (b) LBIC image of an industrial mc solar cell at 940 nm, (c) ILIT-based J_{sc}, measured at 940 nm, (d) DLIT-based J_{sc}, fitted to 940 nm LBIC, all taken from [31]

The short circuit current density J_{sc} is another important local solar cell parameter, whose definition is also out of question. In many PL and DLIT evaluation methods a homogeneous J_{sc} equivalent to its global value is assumed, but in reality this is not the case. Low lifetime regions generate a lower J_{sc}, which has to be regarded in any local efficiency analysis. The classical way to image J_{sc} is light beam-induced current (LBIC) mapping. This is a sequential method, often needing hours ho obtain a high resolution image. It is also not easy to measure an AM 1.5 LBIC image, see [27]. Therefore alternative J_{sc} imaging methods are desirable. Recently a PL evaluation method was proposed, which also lead to a J_{sc} image [28]. However, also this method was based on the model of independent diodes and therefore has to be considered as not correct. Indeed, a recent comparison of this and other methods to LBIC has proven this inaccuracy [29]. This paper also discusses another method based on illuminated lock-in thermography (ILIT), which was proposed by Fertig et al. [30], as well as a method based on DLIT introduced by Breitenstein et al. [31]. The ILIT-based method relies on measuring the thermalization heat of the photocurrent flowing across the pn-junction under weak reverse bias, where no carrier multiplication is expected yet. The same measurement principle was used already earlier for measuring the local avalanche multiplication factor [32]. Since for this ILIT-J_{sc} imaging two quite similar ILIT images are subtracted from each other (typically one for 0 V and one for -1 V), it is useful to perform here LIT with local emissivity correction, which is provided e.g. in the PV-LIT system by InfraTec [33]. Since for applying this method permanent (not pulsed) illumination is sufficient, a conventional solar simulator can be used for realizing AM 1.5 illumination.

The advantage of the DLIT-based method for imaging J_{sc} [31], compared to the ILIT-based method [30], is that it needs no homogeneous illumination. If there was a DLIT investigation of a cell in the past, this method can even be applied afterwards. This method is based on the fact that the saturation current density J_{01} is a local measure of the recombination properties of the bulk and the surfaces. This holds also under short-circuit condition, where J_{sc} is measured. In this method it is assumed that the amount of photo-generated carriers per time and area (the so-called generation current density J_{gen}) is homogeneous across the area and that, depending on the local lifetime properties, a certain current density $J_{rec,sc}(x,y)$ is lost at short circuit by recombination. Hence, $J_{sc}(x,y) = J_{gen} - J_{rec,sc}(x,y)$ holds. By performing PC1D simulations it has been found that, for low J_{01}, $J_{rec,sc}$ depends linearly on J_{01} and for high J_{01} slightly non-linearly, see Fig. 11 (a). Therefore $J_{sc}(J_{01})$ has been fitted empirically to a quadratic function with three parameters A, B, and C:

$$J_{rec,sc}(x,y) = J_{gen} - J_{sc} = AJ_{01}(x,y) - BJ_{01}^2(x,y) - C \qquad (7)$$

The parameter B describes the degree on nonlinearity for higher J_{01}, and the parameter C governs the average value of J_{sc}. If this average value $\langle J_{sc} \rangle$ is known, e.g. from flasher measurements, we may replace parameter C and the final result has only two parameters:

$$J_{sc}(x,y) = < J_{sc} > + \sum_{i=1}^{N} \frac{AJ_0(x,y) - BJ_0^2(x,y)}{N} - AJ_{01}(x,y) + BJ_{01}^2(x,y) \quad (8)$$

For a typical industrial solar cell the parameters $A = 2*10^9$ and $B = 2*10^{20}$ cm^2/A have been fitted to AM 1.5 and $A = 3.5*10^9$ and $B = 2{,}5*10^{20}$ cm^2/A to 940 nm LBIC results [31]. Fig. 11 (b), (c), and (d) show images of LBIC-J_{sc}, ILIT-J_{sc}, and DLIT-J_{sc} of an industrial solar cell, all measured at a wavelength of 940 nm, from [29,31]. We see that the correlation between these images is good. These methods may provide the base for a more realistic simulation of the local efficiency of solar cells, compared to previous attempts, which relied on the assumption of a homogeneous J_{sc} [4,7]. The DLIT-based J_{sc} imaging method is already implemented in the latest version of the "Local I-V 2" software for evaluating DLIT images and performing a local cell efficiency analysis, which is based on [3,4] and is available [34]. The limitation of this method is that it needs the two parameters A and B, which may depend on the individual solar cell structure [31].

5. Conclusions

In this contribution some older and several new developments regarding the imaging of essential local solar cell parameters, like the local series resistance, the saturation current density J_{01}, and the short circuit current density J_{sc}, are reviewed. Most part of this work regards the local series resistance. It is found that there are several different definitions of the local series resistance, which can be measured by various methods. However, none of the previous definitions can be used to describe a solar cell both in the dark and under illumination. Most authors define the local series resistance as the local voltage drop between a certain position and the busbars, divided by the local diode current density. This definition is equivalent to the application of the model isolated diodes, which assumes that each elementary diode (pixel) is connected to the terminals by its individual series resistance. However, in reality most part of the series resistance is due to horizontal currents flowing in the gridlines and in the emitter, hence it is distributed. There are some CELLO- and PL-based attempts to measure the local series resistance regarding its distributed nature, but these definitions cannot be used in the dark case and do not deliver any direct information to the local value of J_{01}. Here a proposal is made how to fit experimental imaging results (DLIT and EL, both performed at the same bias) to the components of a 2-dimensional finite element equivalent circuit of a solar cell. This fit leads to meaningful images of the local J_{01}, of the horizontal grid resistance (R_{grid}, including grid breakage sites), and of the grid contact resistance $R_{contact}$. Hence, in this concept the effective local series resistance is described by two different resistance images. Though this method still needs to be improved, it is hoped that by this concept the solar cell can be described in the dark and under illumination by one and the same series resistance data set, resulting from experimental imaging results.

In the second part of this work the question how to measure the correct J_{01} image is answered. Until now DLIT- and PL-based J_{01} images did not agree with each other. By performing one-dimensional diode chain simulations and 2-dimensional model diode simulations it is found that all previous PL-based J_{01} images systematically underestimated local maxima of J_{01}. The reason is the too simple model of independent diodes applied in these methods. Luminescence methods only can measure local diode voltages (chemical potentials), but no local currents. These have to be derived from the voltage distribution, e.g. by assuming an equivalent circuit like the independent diode model. Since this model does not hold, all previously luminescence-measured current densities are obviously wrong. DLIT, on the other hand, measures the local current more directly by measuring the locally dissipated heat. Our simulations have shown that, apart from the inevitable thermal blurring, DLIT images J_{01} correctly. These investigations confirm and prove earlier [10] and most recent statements [35] that, for performing a comprehensive local analysis of inhomogeneous solar cells and modules, the combined application of both thermal and luminescence imaging methods is indispensable.

Finally, two new methods for imaging J_{sc} by ILIT and DLIT methods are introduced. Both methods are found to be useful. The DLIT-based method has the advantage not to need a homogeneous illumination source, and it can be applied even after a DLIT measurement has been made. On the other hand, it relies on an empirical formula and needs two fitted parameters, in contrast to the ILIT-based method.

The author is grateful to J. Bauer and F. Frühauf (MPI Halle), S. Rißland (now Calyxo, Bitterfeld-Wolfen), and D. Hinken and K. Bothe (ISFH Hamelin) for experimental cooperation and performing simulations, to J.-M. Wagner (Kiel University) for helpful discussions, and to InfraTec (Dresden [33]) for providing the LIT system used for most of these investigations. This work was supported by the German Ministry for Economic Affairs and Energy under Grant No. 0325763D (SolarLIFE) and by industrial partners.

References

[1] O. Breitenstein, Understanding the current-voltage characteristics of industrial crystalline silicon solar cells by considering inhomogeneous current distributions, Opto-Electronics Review **21**, 259-282 (2013).

[2] O. Breitenstein, W. Warta, and M. Langenkamp, Lock-in Thermography - Basics and Use for Evaluating Electronic Devices and Materials, 2nd Edition, Springer 2010.

[3] O. Breitenstein, Nondestructive local analysis of current-voltage characteristics of solar cells by lock-in thermography, Solar Energy Mat. & Solar Cells **95** (2011) 2933-2936.

[4] O. Breitenstein, Local efficiency analysis of solar cells based on lock-in thermography, Solar Energy Mat. & Solar Cells **107** (2012) 381-389.
[5] M. Glatthaar, J. Haunschild, M. Kasemann, J. Giesecke, W. Warta, and St. Rein, Spatially resolved determiunation of dark saturation current and series resistance of silicon solar cells, Physica Status Solidi RRL **4** (2010) 13-15.
[6] M. Glatthaar, J. Haunschild, R. Zeidler, M. Demant, J. Greulich, B. Michel, W. Warta, and R. Preu, Evaluating luminescence based voltage images of solar cells, J. Appl. Phys. **108** (2010) 014501.
[7] C. Shen, H. Kampwerth, M. Green, T. Trupke, J. Carstensen, and A. Schütt, Spatially resolved photoluminescence imaging of essential silicon solar cell parameters and comparison with CELLO measurements, Solar Energy Mat. & Solar Cells **109** (2013) 77-81.
[8] J. Carstensen, A. Schütt, G. Popkirov, and H. Föll, CELLO measurement technique for local identification and characterization of various types of solar cell defects, Physica Status Solidi **C8** (2011) 1342-1346.
[9] J.-M. Wagner, J. Carstensen, A. Berhane, A. Schütt, and H. Föll, Serial resistance analysis with the shaded luminescence technique, Proc. 26th Eur. Photovoltaic Solar Energy Conference, Hamburg 2011, pp. 1569-1575.
[10] O. Breitenstein, J. Bauer, K. Bothe, D. Hinken, J. Müller, W. Kwapil, M.C. Schubert, and W. Warta, Can luminescence imaging replace lock-in thermography on solar cells?, IEEE J-PV **1** (2011) 159-167.
[11] O. Breitenstein, C. Shen, H. Kampwerth, and M.A. Green, Comparison of DLIT- and PL-based local solar cell efficiency analysis, Energy Procedia 38 (2013) 2-12.
[12] O. Breitenstein, J. Carstensen, A. Schütt, and J.-M. Wagner, Comparison of local solar cell efficiency analysis performed by DLIT and CELLO, Proc. 28th EU PVSEC, Paris 2013, pp. 1538-1544.
[13] P.E. Mijnarends, G.J.M. Janssen, W.C. Sinke, The effect of material inhomogeneities on the characteristics of semicrystalline silicon solar cells: the second diode, Solar Energy Mat. & Solar Cells **33** (1994) 345-360.
[14] T. Trupke, E. Pink, R.A. Bardos, and M.D. Abbott, Spatially resolved series resistance of silicon solar cells obtained from luminescence imaging, Appl. Phys. Lett. **90** (2007) 093506.
[15] G. Araujo, A. Cuevas, and J.M. Ruiz, The effect of distributed series resistance on the dark and illuminated current-voltage characteristics of solar cells, IEEE Transactions on Electron Devices **33** (1986) 391-401.
[16] K. Bothe. and D. Hinken, Quantitative Luminescence Characterization of Crystalline Silicon Solar Cells, in "Advances in Photovoltaics, Volume 2" (ed. G.P. Willeke and E.R. Weber), Academic Press (Burlington), Elsevier (2013), pp. 299 ff.
[17] K. Ramspeck, K. Bothe, D. Hinken, B. Fisher, J. Schmidt, and R. Brendel, Recombination current and series resistance imaging of solar cells by combined luminescence and lock-in thermography, Appl. Phys. Lett. **90** (2007) 153502.
[18] O. Breitenstein and S. Rißland, A two-diode model regarding the distributed series resistance, Solar Energy Mat. & Solar Cells **110** (2013) 77-86.
[19] J. Haunschild, M. Glatthaar, M. Kasemann, S. Rein, and E.R. Weber, Fast series resistance imaging for silicon solar cells using electroluminescence, Physica Status Solidid RRL **3** (2009) 227-229.
[20] J. Wong, Griddler: Intelligent computer aided design of complex solar cells, Proc. 40th IEEE PVSC, Tampa 2013, pp. 933-938.
[21] O. Breitenstein, J. Bauer, D. Hinken, and K. Bothe, The reliability of thermography- and luminescence-based series resistance and saturation current density imaging, Solar Energy Mat. & Solar Cells **137** (2015) 50-60.
[22] O. Breitenstein, J. Bauer, D. Hinken, and K. Bothe, Towards an improved Laplacian-based photoluminescence image evaluation method, Solar Energy Mat. & Solar Cells, in print.
[23] P. Nenzi, Ngspice circuit simulator release 26, 2014, http://ngspice.sourceforge.net/.
[24] U. Rau, V. Huhn, L. Stoicescu, M. Schneemann, Y. Augarten, A. Gerber, and B.E. Pieters, Photocurrent collection efficiency mapping of a silicon solar cell by a differential luminescence imaging technique. Appl. Phys. Lett. **105** (2014) 163507.
[25] J. Wong and M.A. Green, From junction to terminal: Extended reciprocity relations in solar cell operation, Phys. Rev. B 85 (2012) 235205.
[26] D. Walther, A. Fell, E. Franklin, D. Macdonald, B. Mitchell, and Th. Trupke, The impact of silicon CCD photon spread on quantitative analyses of luminescence images, IEEE J-PV **4** (2014) 368-373.
[27] M. Padilla, B. Michl, B. Thaidigsmann, W. Warta, and M.C. Schubert, Short-circuit current density mapping for solar cells, Solar Energy Mat. & Solar Cells **120** (2014) 282-288.
[28] O. Breitenstein, H. Höffler, and J. Haunschild, Photoluminescence image evaluation of solar cells based on implied voltage distribution, Solar Energy Mat. & Solar Cells **128** (2014) 296-299.
[29] F. Fertig, M. Padilla, O. Breitenstein, H. Höffler, I. Geisermeyer, M.C. Schubert, and S. Rein, Short-circuit current density imaging methods for silicon solar cells, Talk at 5th SiliconPV, Konstanz 2015, to appear in Energy Procedia.
[30] F. Fertig, J. Greulich, and S. Rein, Spatially resolved determination of the short-circuit current density of silicon solar cells via lock-in thermography, Appl. Phys. Lett. **104** (2014) 201111.
[31] O. Breitenstein, F. Fertig, and J. Bauer, An empirical method for imaging the short circuit density in silicon solar cells based on dark lock-in thermography, Solar Energy Mat. & Solar Cells, in print.
[32] O. Breitenstein, J. Bauer, J.-M. Wagner, and A. Lotnyk, Imaging physical parameters of pre-breakdown sites by lock-in thermography techniques, Progress in Photovolt: Research and Applications **16** (2008) 679-685.
[33] www.infratec.eu
[34] www.maxplanckinnovation.de/en
[35] A. Gerber, V. Huhn, T.M.H. Tran, M. Siegloch, Y. Augarten, B.E. Pieters, and U. Rau, Advanced large area characterization of thin-film solar modules by electroluminescence and thermography techniques. Solar Energy Mat. & Solar Cells **135** (2015) 35-42.